

Electronic structures of (In,Ga)As/GaAs quantum dot molecules made of dots with dissimilar sizes

Lixin He¹ and Alex Zunger²

¹Key Laboratory of Quantum Information, University of Science and Technology of China, Hefei, Anhui 230026, Peoples Republic of China

²National Renewable Energy Laboratory, Golden, Colorado 80401, USA

(Dated: February 8, 2020)

Using single-particle pseudopotential and many-particle configuration interaction methods, we compare various physical quantities of (In,Ga)As/GaAs quantum dot molecules (QDMs) made of dissimilar dots (heteropolar QDMs) with QDMs made of identical dots (homopolar QDMs). The calculations show that the electronic structures of hetero-QDMs and homo-QDMs differ significantly at large inter-dot distance. In particular (i) Unlike those of homo-QDMs, the single-particle molecular orbitals of hetero-QDMs convert to dot localized orbitals at large inter-dot distance. (ii) Consequently, in a hetero-QDM the bonding-antibonding splitting of molecular orbitals at large inter-dot distance is significantly larger than the electron hopping energy whereas for homo-QDM, the bonding-antibonding splitting is very similar to the hopping energy. (iii) The asymmetry of the QDM increases significantly the double occupation for the two-electron ground states, and therefore affects the degree of entanglement of the two electrons. Calculations on the electron addition energies $\Delta(N-1, N)$ as a function of the number N of electrons show that QDMs have only one peak in strong and weak coupling region at $N-1= 2, 4$ respectively, while in intermediate coupling region both addition energy peaks are seen, indicating new molecular phases emerge in this region.

PACS numbers: 73.22.GK, 03.67.Mn, 85.35.-p

I. INTRODUCTION

Vertically coupled quantum dots^{1,2} obtained via epitaxial growth provide a potential scheme for scalable nano-structures for quantum computing. In this scheme, two coupled quantum dots are used as a basic logic gate, via the entanglement of one exciton³ or two electronic spins.⁴ This proposal for gate operations, requires knowledge of the detailed physical properties of the “quantum gate” made of two quantum dots. Significant progress has been recently made^{5,6} using quantum dot molecules made of very large ($\sim 500 - 1000 \text{ \AA}$) electrostatically confined dots. The limit of large quantum confinement, however, requires working with ($200 \times 30 \text{ \AA}$) self-assembled QDMs. So far, most experiments on self-assembled QDM are optical,³ and most theories are based on continuum models, such as effective mass approximations.³ These simple models ignore or drastically simplify important real material properties such as strain, atomistic symmetries and crystal structural effects, band coupling etc. Recent studies⁷ show that simplification of such important effects may lead to qualitative changes in fundamental physics of the QDMs.

Previously, we have studied homopolar QDMs made of two identical quantum dots, using single-particle pseudopotential method and many-particle configuration interaction method.^{8,9} We have studied electron localiza-

tion, double occupation rate and two-electron entanglement using a new formula for measuring the degree of entanglement formula for two *indistinguishable* fermions. We found that even geometrically identical dots in the QDMs lead to electronic asymmetry due to the strain effects. However, experimentally it is hard to control the shape, size and compositions of individual dots within the QDMs, so in practice, the QDMs are never made of identical dots. Actually, the top dots are tend to be larger than the bottom dots due to the strain effects.^{1,2} Indeed, the measured difference in exciton energy due to dot-size difference is about 4 meV¹⁰ for two vertically coupled dots that are 20 nm apart. Sometimes, the two dots are intentionally grown different so that they can be addressed separately.¹¹ To provide quantitative comparison to experiments, considering the effects that asymmetry of quantum dots within the molecule, we studied the QDMs made of (In,Ga)As/GaAs quantum dots of different sizes (hetero-polar QDM).

In this paper, we study systematically the electronic properties of hetero-QDMs, including their single-particle molecular orbitals, many-particle states, double occupation and entanglement of two-electrons, and compare them to those of homo-QDMs. We found that while at *short* inter-dot distance, the electronic properties of hetero-QDM and homo-QDM are similar, they differ significantly at *large* inter-dot distance. This difference may have substantial impact in implementation of quantum

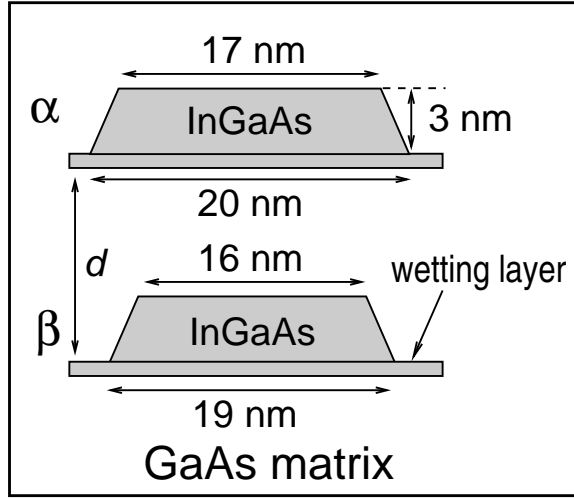


FIG. 1: The geometry used in this work for quantum dot molecules made of dissimilar dots. We denote the (isolated) top dot “ α ” and the (isolated) bottom dot “ β ”. Each dot has the shape of a truncated cone. The inter-dot distance is measured from wetting layer to wetting layer.

gates.

II. METHODS

Figure 1 shows the geometry of a hetero-QDM, consisting a pair of 3 nm tall InAs dots in the shape of truncated cones, grown on two-dimensional InAs wetting layers, embedded in a GaAs matrix. The inter-dot separation d is defined as the distance between the wetting layers of top and bottom dots. We choose the base diameter of top dots (labeled as α) to be 20 nm, and that of the bottom dots (labeled as β) to be 19 nm, mimicking to the fact that experimentally the top dots are slightly larger than the bottom dots.^{1,2,10} The composition of the dots vary from $\text{In}_{0.5}\text{Ga}_{0.5}\text{As}$ at their bases to pure InAs at their top, as determined in Ref. 3. We denote the dot molecules made of dissimilar dots α and β as $M_{\alpha\beta}$. In previous calculations, we studied the QDMs made of two identical, pure InAs/GaAs dots^{8,9}, which have base diameter=12 nm, and height=2 nm. We denote the single dot as dot γ , and the QDM as $M_{\gamma\gamma}$. Dot γ is much smaller than dots α and β . We use $M_{\gamma\gamma}$ here as references to show that the *general* conclusions on electronic structures of homo- vs. hetero-QDM do not rely on the particular choice of the sizes and compositions of the QDM. To isolate effects due to the homopolar *vs* heteropolar QDM, we also constructed a QDM called $M_{\alpha'\alpha'}$ made of identical dots, each being the average of dots α and β in the heteropolar dot molecule. Comparison of $M_{\alpha\beta}$ and $M_{\alpha'\alpha'}$ will be discussed in Sec. IV B and V.

The single-particle energy levels and wavefunctions of $M_{\alpha\beta}$ and $M_{\gamma\gamma}$ are obtained by solving the Schrödinger equations in a pseudopotential scheme,

$$\left[-\frac{1}{2} \nabla^2 + V_{\text{ps}}(\mathbf{r}) \right] \psi_i(\mathbf{r}) = \epsilon_i \psi_i(\mathbf{r}) , \quad (1)$$

where the total electron-ion potential $V_{\text{ps}}(\mathbf{r})$ is a superposition of local, screened atomic pseudopotentials $v_{\alpha}(\mathbf{r})$, and a nonlocal spin-orbit potential V_{so} i.e., $V_{\text{ps}}(\mathbf{r}) = \sum_{n,\alpha} v_{\alpha}(\mathbf{r} - \mathbf{R}_{n,\alpha}) + V_{\text{so}}$. The atomic position $\{\mathbf{R}_{n,\alpha}\}$ is obtained from minimizing the total bond-bending and bond-stretching energy using the Valence Force Field (VFF) model.^{12,13} The atomistic pseudopotentials v_{α} ($\alpha = \text{In}, \text{Ga}, \text{As}$) are fitted to the physically important quantities of bulk InAs and GaAs, including band energies, band-offsets, effective masses, deformation potentials and alloy bowing parameters, etc.¹⁴ Because for electrons the spin-orbit coupling is extremely small in the InAs/GaAs quantum dots, we ignored this effect. In general, including the spin-orbit coupling effect will introduce mixture of different total spin states. Equation (1) is solved in the basis of $\{\phi_{m,\vec{\epsilon},\lambda}(\mathbf{k})\}$ of Bloch orbitals of band index m and wave vector \mathbf{k} of material λ (= InAs, GaAs), strained uniformly to strain $\vec{\epsilon}$ following Ref. 15.

The Hamiltonian of interacting electrons can be written as,

$$H = \sum_{i\sigma} \epsilon_{\alpha} \hat{\psi}_{i\sigma}^{\dagger} \hat{\psi}_{i\sigma} + \frac{1}{2} \sum_{ijkl} \sum_{\sigma,\sigma'} \Gamma_{kl}^{ij} \hat{\psi}_{i\sigma}^{\dagger} \hat{\psi}_{j\sigma'}^{\dagger} \hat{\psi}_{k\sigma'} \hat{\psi}_{l\sigma} , \quad (2)$$

where $\hat{\psi}_{i\sigma}(\mathbf{r}) = c_{i\sigma} \psi_{i\sigma}(\mathbf{r})$ is the field operator, whereas $c_{i\sigma}$ is a fermion operator. $\psi_i = \sigma_u, \sigma_g, \pi_u, \pi_g$ are the single-particle eigenfunctions of the *i-th molecular orbital*, and $\sigma, \sigma' = 1, 2$ are spin indices. The Γ_{kl}^{ij} are the Coulomb integrals between molecular orbitals ψ_i, ψ_j, ψ_k and ψ_l ,

$$\Gamma_{kl}^{ij} = \int \int d\mathbf{r} d\mathbf{r}' \frac{\psi_i^*(\mathbf{r}) \psi_j^*(\mathbf{r}') \psi_k(\mathbf{r}') \psi_l(\mathbf{r})}{\epsilon(\mathbf{r} - \mathbf{r}') |\mathbf{r} - \mathbf{r}'|} . \quad (3)$$

The $J_{ij} = \Gamma_{ji}^{ij}$ and $K_{ij} = \Gamma_{ij}^{ij}$ are diagonal Coulomb and exchange integrals respectively. The remaining terms are called off-diagonal or scattering terms. All Coulomb integrals are calculated numerically from atomistic wavefunctions.¹⁶ We use a phenomenological, position-dependent dielectric function $\epsilon(\mathbf{r} - \mathbf{r}')$ to screen the electron-electron interaction.¹⁶ The many-particle problem of Eq.(2) is solved via the CI method, by expanding the N -electron wavefunction in a set of Slater determinants, $|\Phi_{e_1, e_2, \dots, e_N}\rangle = c_{e_1}^{\dagger} c_{e_2}^{\dagger} \dots c_{e_N}^{\dagger} |\Phi_0\rangle$, where $c_{e_i}^{\dagger}$ creates an electron in the state e_i . The ν -th many-particle wavefunction is then the linear combinations of the determinants,

$$|\Psi_{\nu}\rangle = \sum_{e_1, e_2, \dots, e_N} A_{\nu}(e_1, e_2, \dots, e_N) |\Phi_{e_1, e_2, \dots, e_N}\rangle . \quad (4)$$

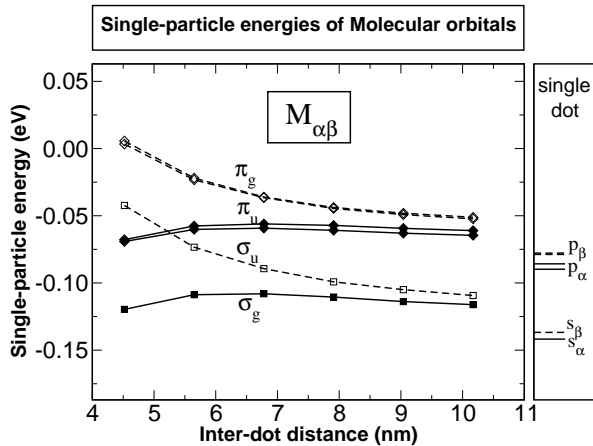


FIG. 2: Left panel: The single-particle energy levels of molecular orbitals *vs.* inter-dot distance. Right panel: The electron single-particle energy levels of the isolated dots α and β .

For the two-electron problems, our calculations include all possible Slater determinants of six confined molecular orbitals.

III. BASIC ELECTRONIC STRUCTURES AT THE SINGLE-PARTICLE LEVEL

A. Double-dot molecular orbitals

We first show the electronic structure of isolated dots α and β . The single-dot electron s and p levels of dots α and β are shown on the right panel of Fig. 2. We see that the s - p energy spacing of dot α is $\epsilon(p_\alpha) - \epsilon(s_\alpha) = 52$ meV and that of dot β is $\epsilon(p_\beta) - \epsilon(s_\beta) = 59$ meV, compared to 105 meV of dot γ (not shown). The energy level of s_β , is slightly (~ 6 meV) higher than s_α , because dot β is smaller than dot α and therefore has larger confinement. The p levels of all dots have a small energy splitting due to the underlying atomistic symmetry, e.g., $\delta\epsilon(p_\alpha) = 6$ meV, and $\delta\epsilon(p_\beta) = 1$ meV. We further calculated the the fundamental exciton energy of dot α , $E_X(\alpha) = 1153$ meV, and that of dot β , $E_X(\beta) = 1159$ meV. The energy difference in exciton of dots α and β is about 6 meV, in agreement with experiment.¹⁰

When two dots α and β couple, the bonding and anti-bonding ‘‘molecular orbitals’’ ensue from the single-dot orbitals. The energy levels of molecular orbitals are shown on the left panel of Fig. 2. We show the single-particle levels of molecular orbitals^{8,9} σ_g , σ_u originating from s orbitals, and π_u , and π_g originating from p orbitals. The bonding and anti-bonding splitting $\Delta_\sigma =$

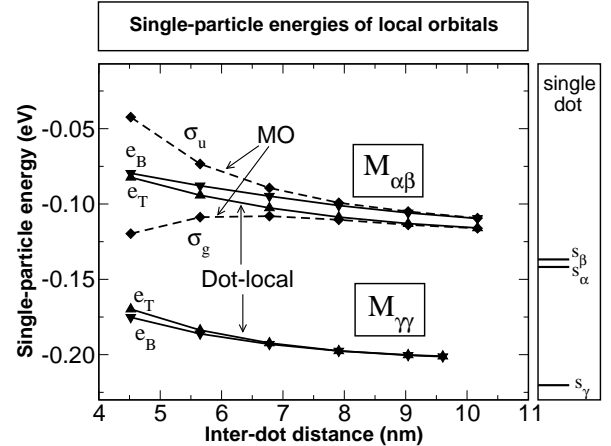


FIG. 3: Left panel: The energy levels of dot-localized orbitals (solid lines) for QDMs $M_{\alpha\beta}$ and $M_{\gamma\gamma}$. e_T and e_B denote the s orbitals of the top and bottom dots respectively. The molecular orbitals energy levels σ_g and σ_u (dashed lines) are shown for dot molecules $M_{\alpha\beta}$. Right panel: s levels of isolated dots α , β and γ .

$\epsilon(\sigma_u) - \epsilon(\sigma_g)$ and $\Delta_\pi = \epsilon(\pi_g) - \epsilon(\pi_u)$ increase with the decrease of inter-dot distance, because the coupling between the top and bottom dots gets stronger. This picture is similar to what we obtained for homo-QDMs. However, there is an important difference between the homo-QDMs and hetero-QDMs: in the former case, the bonding and anti-bonding splitting Δ_σ and Δ_π decay to zero at large inter-dot distance (Fig.1b in Ref.8), while in the later case, Δ_σ and Δ_π tend to constants ($\Delta_\sigma \sim 7$ meV, $\Delta_\pi \sim 10$ meV here), because the molecular orbitals gradually convert at large inter-dot distance to single dot energy levels, e.g. the σ_g levels convert to top dot s orbitals, and σ_u convert to bottom dot s orbitals, therefore the energy splitting between the first and second molecular states at large distances is approximately the energy difference between s orbitals of the top and bottom dots, i.e., $\Delta_\sigma \sim \epsilon(s_\beta) - \epsilon(s_\alpha) \neq 0$ for $M_{\alpha\beta}$.

Figure 2 shows that at inter-dot distance $d = 10$ nm, the molecular orbital levels are about 25 meV higher than the isolated dot levels, although the direct electronic coupling between two dots is much smaller than this quantity. This energy shift results from the long range strain effects experienced by one dot due to the presence of the second dots. This effect is missed in EMA-type model calculations,¹⁷ which ignore strain effects.

B. Single dot-localized orbitals

The above discussions pertain to the basis of double-dot molecular orbitals. An alternative way to study

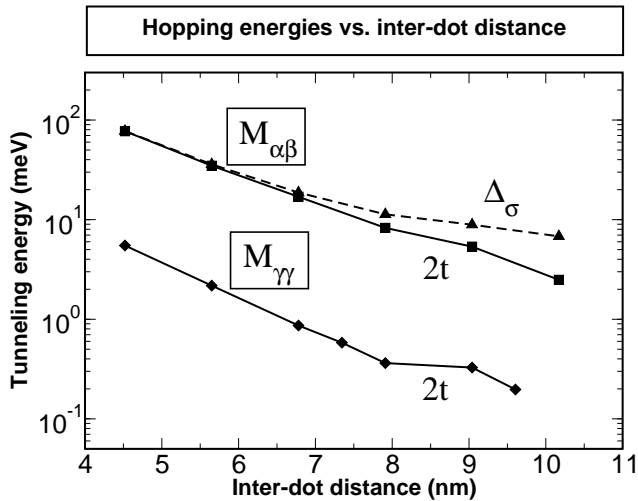


FIG. 4: The inter-dot hopping energy $2t$ (solid lines) of hetero-QDM $M_{\alpha\beta}$ and homo-QDM $M_{\gamma\gamma}$. We also show the bonding-antibonding splitting Δ_σ of $M_{\alpha\beta}$.

QDMs is to use a dot-localized basis. We have demonstrated^{8,9} that dot-localized orbitals can be a useful tool to analyze the QDM physics, including the electron double occupation, and two-electron entanglement.

Dot-localized orbitals χ_η can be obtained from a unitary rotation of molecular orbitals, i.e.,

$$\chi_\eta = \sum_{i=1}^N \mathcal{U}_{\eta,i} \psi_i, \quad (5)$$

where, ψ_i is the i -th molecular orbital, and \mathcal{U} is a unitary matrix, i.e., $\mathcal{U}^\dagger \mathcal{U} = I$. We choose the unitary matrices \mathcal{U} that maximize the total orbital self-Coulomb energy.^{9,18} The procedure of finding \mathcal{U} is described in the Appendix B of Ref.9. As we will show below these dot-localized orbitals χ_η have the advantage of being only weakly dependant to the inter-dot coupling. This invariance may provide simplified pictures for qualitatively understanding of the QDM physics.

1. Single-particle energies of dot-localized orbitals

The single-particle levels of dot-localized orbitals and the hopping (or tunneling) term between two dots can be obtained from

$$e_\eta = \langle \chi_\eta | \hat{H}_0 | \chi_\eta \rangle = \sum_i \mathcal{U}_{\eta,i}^* \mathcal{U}_{\eta,i} \epsilon_i, \quad (6)$$

$$t_{\eta_1 \eta_2} = \langle \chi_{\eta_1} | \hat{H}_0 | \chi_{\eta_2} \rangle = \sum_i \mathcal{U}_{\eta_1,i}^* \mathcal{U}_{\eta_2,i} \epsilon_i, \quad (7)$$

where, ϵ_i is the single-particle energy of i -th molecular orbital and $\hat{H}_0 = \sum_{i\sigma} \epsilon_i \hat{\psi}_{i\sigma}^\dagger \hat{\psi}_{i\sigma}$ is the single-particle Hamiltonian. Figure 3 depicts the single-particle levels e_T and e_B of the dot-localized orbitals of both top and bottom dots, for inter-dot distances d in the range from 4 nm to 10 nm. (Here, we denote the top dot T and the bottom dot B , to distinguish them from isolated dots α and β). At large d , the energy difference $e_B - e_T \sim 6$ meV, is close to the value of difference $\epsilon(s_\beta) - \epsilon(s_\alpha)$ between s orbitals of isolated dots α, β . This energy difference gets smaller when the two dots move closer, because the energy levels of the top dot rise faster than those of bottom dots due to the strain asymmetry. These strain effects are consistent with the results of homo-QDMs $M_{\gamma\gamma}$, also shown in Fig. 3, whose e_T is almost degenerate with e_B at large d , but is higher in energy than e_B at smaller d . To see the relations between molecular orbitals and dot-localized orbitals, we plot in Fig. 3 the energies of molecular orbitals σ_u and σ_g in dashed lines. As we see, for $d > 9$ nm, the dot-localized e_B state is almost identical to the molecular orbital σ_u , while e_T merges with σ_g , indicating at large d , molecular orbitals convert to dot-centered orbitals.

The quantity $2t$ measures the coupling strength between the top and bottom dots, and directly determines the two-electron properties such as singlet-triplet splitting in the QDM. We calculate this hopping energy between the s orbitals of top and bottom dots at different inter-dot distances for both $M_{\alpha\beta}$ and $M_{\gamma\gamma}$ in Fig. 4. (We ignore the orbital index “ s ” to simplify the notation.) We find that $2t(M_{\alpha\beta})$ and $2t(M_{\gamma\gamma})$ have similar slopes. However, $2t(M_{\alpha\beta})$ is much larger than $2t(M_{\gamma\gamma})$. This is because dots α and β are alloy dots and the energy barrier between two dots is much smaller the barrier in $M_{\gamma\gamma}$. In general, the quantity $2t$ does not equal to the bonding-antibonding splitting $\Delta_\sigma = \sqrt{\delta^2 + 4t^2}$, where $\delta = \epsilon(e_T) - \epsilon(e_B)$, being the energy difference of s orbitals of the top and bottom dots. For homo-QDMs, where $\delta/2t \ll 1$, we have $2t \sim \Delta_\sigma$. However, for hetero-QDMs, Δ_σ may be significantly different from $2t$, especially at large inter-dot distances, where $\delta/2t \gg 1$, as illustrated in Fig. 4. Experimentally,¹⁹ one usually measures the bonding-antibonding splitting rather than the hopping $2t$. Therefore, to get the hopping energy between two dots, one need to know the energy difference δ of two dots.

2. Coulomb integrals of dot-localized orbitals

The Coulomb integrals in the dot-localized basis can be obtained from Coulomb integrals of molecular orbitals

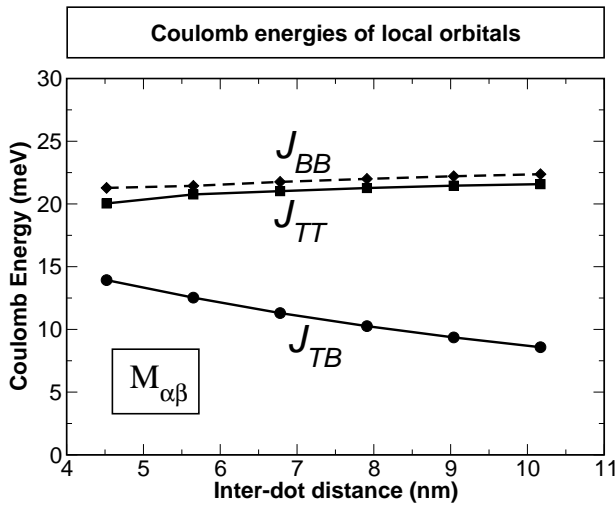


FIG. 5: The Coulomb energies of dot-localized orbitals. J_{TT} and J_{BB} are the s orbital self-Coulomb energies of top and bottom dots respectively, whereas J_{TB} are the Coulomb energies between s orbitals of the top and the bottom dots.

as follows,

$$\tilde{\Gamma}_{\eta_3, \eta_4}^{\eta_1, \eta_2} = \sum_{i, j, k, l} \mathcal{U}_{\eta_1, i}^* \mathcal{U}_{\eta_2, j}^* \mathcal{U}_{\eta_3, k} \mathcal{U}_{\eta_4, l} \Gamma_{k, l}^{i, j}, \quad (8)$$

where $\Gamma_{k, l}^{i, j}$ are the Coulomb integrals in the molecular basis. The direct Coulomb integrals J_{TT} , J_{BB} and J_{TB} are shown in Fig. 5. The Coulomb integrals $J_{TT} \sim J_{\alpha\alpha} = 21.4$ meV and $J_{BB} \sim J_{\beta\beta} = 22.3$ meV, are almost constants at all inter-dot distances, suggesting that the dot-localized orbitals are approximately unchanged for different inter-dot distance d . $J_{\beta\beta} > J_{\alpha\alpha}$, as dot β is smaller than dot α . The inter-dot Coulomb interaction J_{TB} decay slowly as $1/d$. The exchange energies (not shown) between the top and bottom electrons is orders of magnitude smaller than the hopping energy, and therefore can be ignored in practice.

IV. TWO ELECTRONS IN THE DOT MOLECULE

A. Many-body energy states

The two-electron-in-a-QDM problem is of special interest, as it is the prototype of quantum gate using QDMs.⁴ We calculate the two-electron energy levels by the configuration interaction method using Slater determinants constructed from confined molecular orbitals σ_g , σ_u and π_u , π_g , which give 66 configurations in total. The two-electron energies Σ and $^3\Pi_u$ for hetero-QDMs $M_{\alpha\beta}$ are

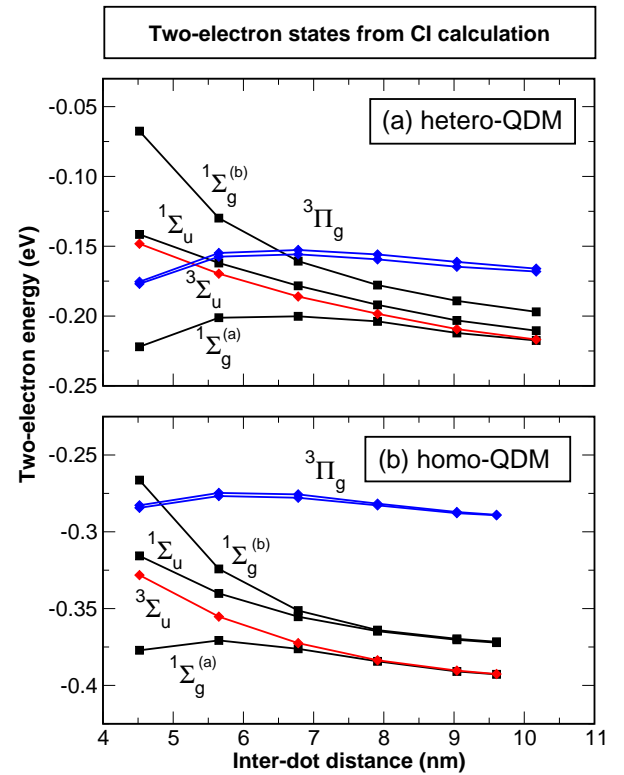


FIG. 6: (Color online) Two-electron states for (a) hetero-QDM $M_{\alpha\beta}$ and (b) homo-QDM $M_{\gamma\gamma}$, including the singlet $^1\Sigma_g^{(a)}$, $^1\Sigma_u$, $^1\Sigma_g^{(b)}$ states and the 3-fold degenerated triplet states $^3\Sigma_u$ as well as two 3-fold degenerated triplet states $^3\Pi_u$.

plotted in Fig. 6(a). To compare with homo-QDMs, we show the two-electron states of $M_{\gamma\gamma}$ in Fig. 6(b). The energy levels of $M_{\alpha\beta}$ are similar to those of $M_{\gamma\gamma}$, in the following way: (i) The order of the CI levels is unchanged, particularly the ground states are still the singlet states $^1\Sigma_g^{(a)}$ at all inter-dot distance; (ii) The trend of each CI level vs. inter-dot distance d is similar to what we obtained for $M_{\gamma\gamma}$. There are also some differences between the hetero-QDMs $M_{\alpha\beta}$ and homo-QDMs $M_{\gamma\gamma}$, especially at larger inter-dot distances. For example, in the homopolar QDMs, the $^1\Sigma_u$ state is almost degenerate with $^1\Sigma_g^{(b)}$ at large inter-dot distance, while in $M_{\alpha\beta}$, $^1\Sigma_g^{(b)}$ is about 13 meV higher than $^1\Sigma_u$ at $d=10$ nm. At large d , $^1\Sigma_u$ and $^1\Sigma_g^{(b)}$ correspond to the states that two electrons localized on the same dots.^{8,9} The energy difference between $^1\Sigma_g^{(b)}$ and $^1\Sigma_u$ is due to the size difference of dots α and β .

The singlet $^1\Sigma_g^{(a)}$ and triplet states $^3\Sigma$ can be used as two qubit states in quantum computing. In a proposed quantum SWAP gate,⁴ the gate operation time $\tau \sim 1/J_{S-T}$, where J_{S-T} being the singlet-triplet energy splitting. The singlet-triplet splitting of $M_{\alpha\beta}$ is shown in Fig. 7 on a semi-log plot. We see that it decay approxi-

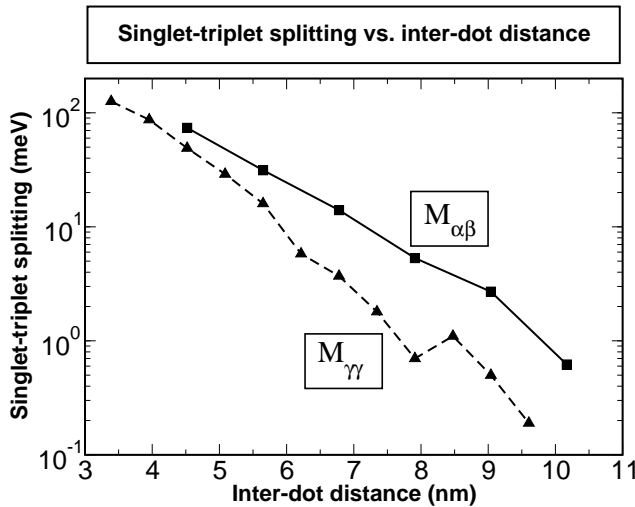


FIG. 7: The singlet-triplet splitting J_{S-T} vs. inter-dot distance for hetero-QDM $M_{\alpha\beta}$ (solid line) and homo-QDM $M_{\gamma\gamma}$ (dashed line).

mately exponentially with the inter-dot distance. We also show in Fig. 7 the singlet-triplet splitting of the homo-QDM case $M_{\gamma\gamma}$. We find that J_{S-T} have similar slope for both $M_{\alpha\beta}$ and $M_{\gamma\gamma}$. However, $J_{S-T}(M_{\alpha\beta})$ is much

larger than $J_{S-T}(M_{\gamma\gamma})$, because the $M_{\alpha\beta}$ are made of alloy dots, and have lower energy barrier than $M_{\alpha\beta}$, which are made of pure InAs/GaAs dots.

B. Double occupation of one of the dots in a QDM

Double occupation means that two electrons occupy the same dot in a QDM. If the double occupation rate is high, the quantum gate operation may fail. The double occupation rate also reflects the localization properties of electrons in the QDM. If the double occupation rate is zero, each dot has one electron, whereas double occupation rate of 1 means that two electrons are always localized on a single dot. When the double occupation rate is 0.5, two electrons are delocalized between two dots. The double occupation can be conveniently analyzed in the dot-localized basis by transforming the CI equations to the dot-localized basis.⁸ In the simplest case, we consider only the “s” orbital for each dot, which give six configurations as follows, $|e_T^\uparrow, e_B^\uparrow\rangle$, $|e_T^\downarrow, e_B^\downarrow\rangle$, $|e_T^\uparrow, e_B^\downarrow\rangle$, $|e_T^\downarrow, e_B^\uparrow\rangle$, $|e_B^\uparrow, e_B^\downarrow\rangle$ and $|e_T^\uparrow, e_T^\downarrow\rangle$. The Hamiltonian in this basis set is,⁹

$$H = \begin{pmatrix} e_T + e_B + J_{TB} - K_{TB} & 0 & 0 & 0 \\ 0 & e_T + e_B + J_{TB} - K_{TB} & 0 & 0 \\ 0 & 0 & e_T + e_B + J_{TB} - K_{TB} & 0 \\ 0 & 0 & 0 & e_T + e_B + J_{TB} - K_{TB} \\ 0 & 0 & 0 & 0 \end{pmatrix} \begin{pmatrix} 0 & 0 & 0 & 0 \\ 0 & 0 & 0 & 0 \\ -K_{TB} & t & t & t \\ -K_{TB} & e_T + e_B + J_{TB} & -t & -t \\ t & -t & 2e_B + J_{BB} & 0 \\ t & -t & 0 & 2e_T + J_{TT} \end{pmatrix}. \quad (9)$$

where $t = t_{TB}$. We ignored in Eq.(9) the off-diagonal Coulomb integrals, which are much smaller than the hopping t .

The calculation of the matrix elements of Eq. 9 is described in Sec.III B. The two electrons can be either both on the top dots, or both on the bottom dots, or one on the top and the other on the bottom dots. We denote by $\{|\chi_{l,p}^\sigma, \chi_{l',p'}^{\sigma'}\rangle\}$ the configuration where one electron is on the l -th orbital of the p dot with spin σ , and the other electron is on the l' -th orbital of the p' dot with spin σ' . Then the double occupation rate $Q_{pp}^{(\nu)}$ in the many-particle state ν is the probability of two electrons occupying the dot p = (T or B) at the same time, i.e.,

$$Q_{pp}^{(\nu)} = \sum_{l\sigma, l'\sigma'} P_\nu(|\chi_{l,p}^\sigma, \chi_{l',p'}^{\sigma'}\rangle), \quad (10)$$

where $P_\nu(\mathcal{C})$ is the weight of the configuration \mathcal{C} in the many-body wave functions of state ν . The total prob-

ability of two electrons being on the *same* dot is then $Q_{\text{tot}}^{(\nu)} = Q_{TT}^{(\nu)} + Q_{BB}^{(\nu)}$ for the ν -th state. We plot Q_{tot} , Q_{TT} and Q_{BB} of state ${}^1\Sigma_g^{(a)}$ for $M_{\alpha\beta}$ in Fig. 8(a). To separate quantitatively the differences in double occupation between homo- and hetero-QDM due to the fact that one is made from identical dots while the other is made from dissimilar dots (without the strain, size and alloy composition effects), we performed calculations on a new “symmetrized” QDM $M_{\alpha'\alpha'}$ made of identical dots, where each of them is the average of dots α and β . We do so by setting $e'_T = e'_B = (e_T + e_B)/2$, and $J'_{TT} = J'_{BB} = (J_{TT} + J_{BB})/2$ in Eq. (9). The calculated double occupations are plotted in Fig. 8(b). We see that (i) For both types of QDMs, $Q_{\text{tot}} \sim 0.5$ at $d \sim 4.5$ nm, meaning that two electrons are delocalized on two dots. For both QDMs, Q_{tot} decays monotonically with the inter-dot distance, and at $d \sim 10$ nm, $Q_{\text{tot}} \sim 0$, meaning that the two electrons are about each localized on one of the two dots.

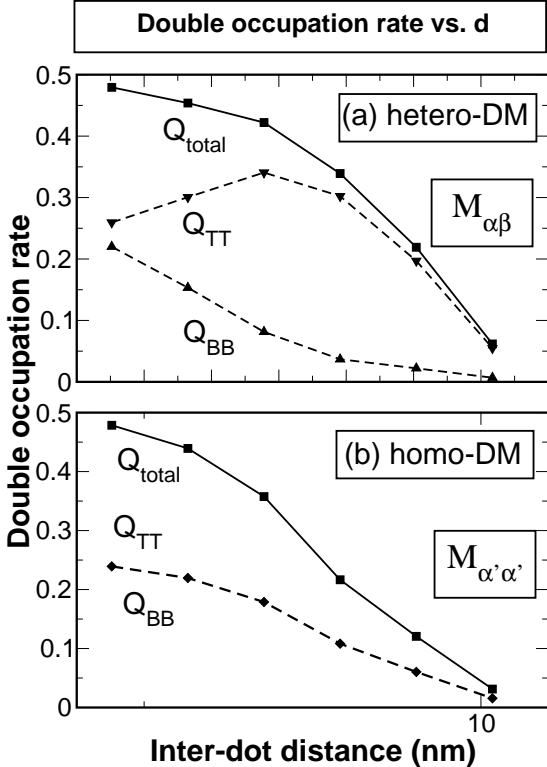


FIG. 8: The double occupation rate of the ground-state singlet ${}^1\Sigma_g^{(a)}$ vs. inter-dot distance for (a) hetero-QDM $M_{\alpha\beta}$ and (b) “symmetrized” homo-QDM $M_{\alpha'\alpha'}$, which has $Q_{\text{TT}}=Q_{\text{BB}}$.

On the other hand, the double occupation of individual dot Q_{TT} and Q_{BB} differ substantially for homo-QDMs and hetero-QDMs:

(ii) For the homo-QDM $M_{\alpha'\alpha'}$, $Q_{\text{BB}} = Q_{\text{TT}}$ and decay monotonically with the inter-dot distances. Q_{BB} and Q_{TT} of $M_{\gamma\gamma}$ have similar features, although Q_{BB} is slightly different from Q_{TT} due to the strain effects.^{8,9} In the hetero-QDMs $M_{\alpha\beta}$, Q_{TT} behaves very differently from Q_{BB} because the effective single-particle energy $e_T < e_B$. Whereas Q_{BB} decays monotonically with the inter-dot distance, Q_{TT} has a maximum at $d \sim 7$ nm. The reason is that at $d \sim 4.5$ nm, the hopping energy t is much larger than $e_B - e_T$, therefore the electrons can overcome the energy barrier between the top and bottom dots and distribute evenly between two dots, leading to $Q_{\text{TT}} \sim Q_{\text{BB}}$. At larger d , $t \ll e_B - e_T$, and the electrons would prefer to localize on the top dots, leading to $Q_{\text{TT}} \gg Q_{\text{BB}}$. Therefore, even when the total double occupation rate drops down, Q_{TT} still increases and reaches the maximum at $d=7$ nm. For $d > 7$ nm, Q_{TT} decays as Q_{tot} decays.

(iii) The asymmetry between two dots increases the total double occupation. In an extreme case, where $e_T \ll e_B$, the two electrons could always localize on the top dots, leading to $Q_{\text{tot}}=Q_{\text{TT}}=1$.

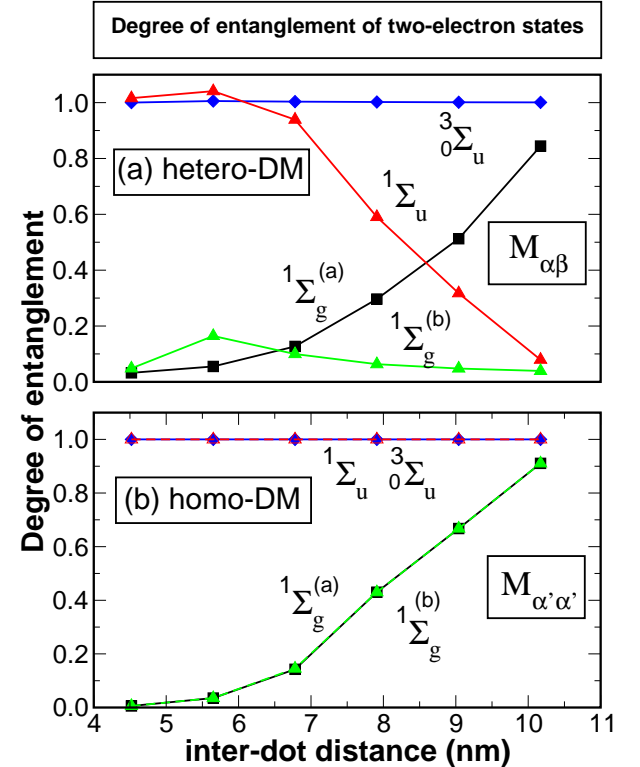


FIG. 9: (Color online) The degree of entanglement of two-electron states ${}^1\Sigma_g^{(a)}$, ${}^1\Sigma_u$, ${}^1\Sigma_g^{(b)}$ and ${}^3\Sigma_u$, in (a) hetero-QDM $M_{\alpha\beta}$ and (b) “symmetrized” homo-QDM $M_{\alpha'\alpha'}$.

V. ENTANGLEMENT

A. Degree of entanglement for two electrons

The degree of entanglement (DOE) is one of the most important quantities for successful quantum gate operations. For *distinguishable* particles such as an electron and a hole, the DOE can be calculated from the Von Neumann-entropy formulation.^{20,21,22,23} However, Von Neumann entropy formulation can not be used directly to calculate DOE for *indistinguishable* particles.^{24,25,26,27,28,29,30} Schliemann et al. proposed a quantum correlation function for two electrons which has similar properties as the DOE.²⁴ However, the generalization of this quantum correlation function to a system that has more than two single-particle levels is complicated. We proposed a DOE measure⁹ for indistinguishable fermions using the Slater decompositions^{24,31} as,

$$\mathcal{S} = - \sum_u z_i^2 \log_2 z_i^2, \quad (11)$$

where, z_i are Slater decomposition coefficients and $\sum_i z_i^2 = 1$. As shown in Ref. 9, the DOE measure Eq.(11) reduces to the usual Von Neumann entropy for *disting-*

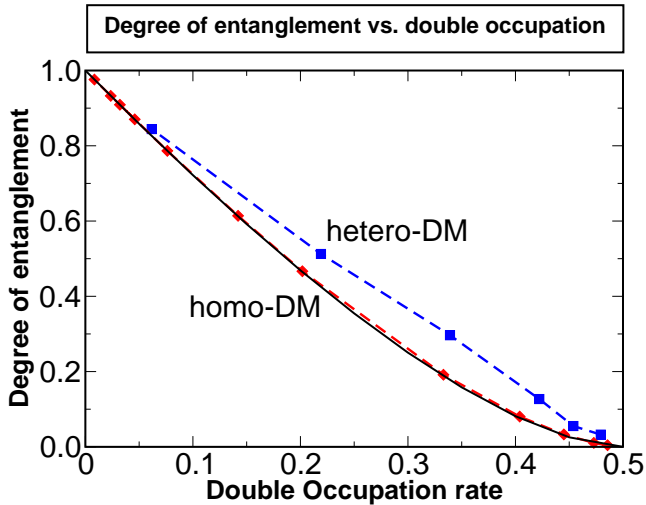


FIG. 10: (Color online) Comparison of the degree of entanglement *vs.* double occupation rate for hetero- and homo-QDMs. The black solid line represents the analytical results of homo-QDMs, and the red dashed line represents the numerical results for homo-QDMs $M_{\alpha'\alpha'}$, and $M_{\gamma\gamma}$, whereas the blue line represents the results for hetero-QDMs $M_{\alpha\beta}$.

guishable particles when the two electrons are far from each other. In Refs. 25,26, a similar DOE measure was defined, which however due to a different normalization condition for z_i was used, does not reduce to the usual Von Neumann entropy even when the two electrons can be distinguished by their sites.

The DOE of Σ states calculated from Eq. (11) for the hetero-QDM $M_{\alpha\beta}$ and the homo-QDM $M_{\alpha'\alpha'}$ are shown in Fig. 9(a) and (b) respectively, both have the following features: (i) $\mathcal{S}(^1\Sigma_g^{(a)})$ is close to zero (unentangled) at $d \sim 4.5$ nm, and close to unity (fully entangled) at $d \sim 10$ nm. (ii) $\mathcal{S}(^3\Sigma)$ is almost unity (fully entangled) at all inter-dot distances.

The above features for $\mathcal{S}(^1\Sigma_g^{(a)})$ and $\mathcal{S}(^3\Sigma)$ are similar to what obtained for homo-QDMs $M_{\gamma\gamma}$. On the other hand, $\mathcal{S}(^1\Sigma_g^{(b)})$ and $\mathcal{S}(^1\Sigma_u)$ are very sensitive to the asymmetry of the QDMs. In general, if the two dots have identical electronic structures (e.g., in the simple Hubbard model), $\mathcal{S}(^1\Sigma_g^{(b)}) = \mathcal{S}(^1\Sigma_g^{(a)})$ and $\mathcal{S}(^1\Sigma_u) = 1$,⁹ as is illustrated in Fig. 9(b) for $M_{\alpha'\alpha'}$. For $M_{\gamma\gamma}$, which is somehow asymmetric due to the strain effects, $\mathcal{S}(^1\Sigma_g^{(b)})$ is very close to $\mathcal{S}(^1\Sigma_g^{(a)})$, and drops down only at large d . In contrast, for $M_{\alpha\beta}$, $\mathcal{S}(^1\Sigma_g^{(b)})$ is small at all inter-dot distances. Similarly, $\mathcal{S}(^1\Sigma_u)$ also behave very differently in homo-QDMs $M_{\alpha'\alpha'}$ and $M_{\gamma\gamma}$ than in hetero-QDM $M_{\alpha\beta}$.

B. Degree of entanglement vs double occupation

Experimentally, it is very hard to measure the DOE of two electrons in the QDM directly, while it is relatively easy to measure the possibility of double occupation. Therefore it would be useful to explore the relation between DOE and the double occupation rate. The triplet states $^3\Sigma$ have negligible double occupation rate due to the Pauli exclusion principle. Here, we discuss the relation between DOE and double occupation rate for the ground state singlet $^1\Sigma_g^{(a)}$. We consider the simplest case, where only “s” orbital in each dot is considered. The ground state singlet $^1\Sigma_g^{(a)}$ wavefunction can be generally written as,

$$\Psi(^1\Sigma_g^{(a)}) = c_1|e_T^\uparrow, e_B^\downarrow\rangle + c_2|e_B^\uparrow, e_T^\downarrow\rangle + c_3|e_T^\uparrow, e_T^\downarrow\rangle + c_4|e_B^\uparrow, e_B^\downarrow\rangle, \quad (12)$$

and $|c_1|^2 + |c_2|^2 + |c_3|^2 + |c_4|^2 = 1$. Alternatively, we have

$$\Psi(^1\Sigma_g^{(a)}) = \sum_{i,j} \omega_{ij}|i\rangle \otimes |j\rangle \quad (13)$$

where,

$$\omega = \begin{pmatrix} 0 & -c_3 & 0 & -c_1 \\ c_3 & 0 & c_2 & 0 \\ 0 & -c_2 & 0 & -c_4 \\ c_1 & 0 & c_4 & 0 \end{pmatrix}, \quad (14)$$

and $|i\rangle, |j\rangle = |e_T^\uparrow\rangle, |e_T^\downarrow\rangle, |e_B^\uparrow\rangle, |e_B^\downarrow\rangle$. We can use Eq. 11 to calculate the DOE, where $z_1^2 = 1/2(1 - \sqrt{1 - 4(c_1c_2 - c_3c_4)^2})$ and $z_2^2 = 1/2(1 + \sqrt{1 - 4(c_1c_2 - c_3c_4)^2})$ are the eigenvalues of $\omega^\dagger \omega$. For a QDM with reflection symmetry, we have $c_1 = c_2$ and $c_3 = c_4$, and therefore $z_1^2 = 1/2(1 - \sqrt{1 - (1 - 4c_3^2)^2})$, and $z_2^2 = 1/2(1 + \sqrt{1 - (1 - 4c_3^2)^2})$. Using the definition of double occupation rate, $Q_{\text{tot}} = c_3^2 + c_4^2$, we have

$$\begin{aligned} z_1^2 &= 1/2(1 - \sqrt{1 - (1 - 2Q_{\text{tot}})^2}), \\ z_2^2 &= 1/2(1 + \sqrt{1 - (1 - 2Q_{\text{tot}})^2}). \end{aligned} \quad (15)$$

The DOE of $^1\Sigma_g^{(a)}$ is calculated by substituting z_1^2 , z_2^2 into Eq. (11). We plot the DOE *vs.* double occupation rate of the above ideal model in Fig. 10 in a black solid line. We also present in the same figure, the DOE of $M_{\alpha\beta}$ and $M_{\gamma\gamma}$ *vs.* double occupation rate. We found that the double occupation dependence of DOE for the homo-QDM $M_{\alpha'\alpha'}$ has perfect agreement with the analytical result, which is also true for $M_{\gamma\gamma}$ even though it has small asymmetry in the molecule due to the strain effects. However, the double occupation dependence of DOE for $M_{\alpha\beta}$ deviates from the ideal case because dots α and β are different.

TABLE I: The ground-state configurations of QDMs $M_{\alpha\beta}$ and $M_{\gamma\gamma}$. We follow the notation of the molecular states from Ref.17.

d (nm)	$M_{\alpha\beta}$				$M_{\gamma\gamma}$			
	4.5	7	8	10	4.0	4.5	5.7	9
N=3	$^2\Pi_u$	$^2\Sigma_u$	$^2\Sigma_u$	$^2\Sigma_u$	$^2\Sigma_u$	$^2\Sigma_u$	$^2\Sigma_u$	$^2\Sigma_u$
N=4	$^3\Sigma_g$	$^1\Sigma_g$	$^1\Sigma_g$	$^1\Sigma_g$	$^1\Sigma_g$	$^1\Sigma_g$	$^1\Sigma_g$	$^1\Sigma_g$
N=5	$^2\Pi_u$	$^2\Pi_u$	$^2\Pi_u$	$^2\Pi_u$	$^4\Sigma_u$	$^2\Pi_u$	$^2\Pi_u$	$^2\Pi_u$
N=6	$^1\Sigma_g$	$^1\Sigma_g$	$^1\Sigma_g$	$^3\Sigma_g$	$^3\Pi_g$	$^3\Sigma_g$	$^3\Sigma_g$	$^1\Sigma_g$

VI. MANY-PARTICLE STATES AND ADDITION ENERGIES

Previously, we have studied the many-particle ground-state configurations and charging/addition energies for single (In,Ga)As QDs.^{32,33} Like the single dot, a dot molecule can also be charged with a few electrons or holes.¹⁹ Using CI methods, we studied the ground state many-particle configurations and charging/addition energies for $N=1$ - 6 electrons in QDMs $M_{\alpha\beta}$ and $M_{\gamma\gamma}$. The ground-state configurations are listed in Table I. The results for one and two electrons are trivial and are therefore not listed in the table. The ground-state configurations show energies crossover of different phases at several inter-dot distances for each number of electrons. These ground-state configurations and energy crossovers are very similar to what Rontani et al¹⁷ obtained using EMA-CI methods, shown in the Fig. 3 of Ref. 17. Certainly, the energy crossover may happen at different inter-dot distances for $M_{\alpha\beta}$, $M_{\gamma\gamma}$, and the dots in Ref. 17, because the parameters of the QDs are different, such as the dot sizes and confining potentials, etc. There are also some subtle differences. For example, in $M_{\gamma\gamma}$, for $N=6$, we found at inter-dot distance ($d \sim 4$ nm), the ground state is $^3\Pi_g$, instead of $^3\Sigma_g$ or $^1\Sigma_g$, although all these states are almost degenerate in energy. More interestingly, at very large d , the ground state of $M_{\gamma\gamma}$ become $^1\Sigma_g$ instead of $^3\Sigma_g$. This is because that in Ref. 17, it is assumed that two Π_u orbitals are degenerate, whereas they actually split, after consideration of the underlying atomistic structures. In a single dot, the electrons have simple ground-state phase diagrams, i.e., the ground state remain unchanged for different dot parameters.^{32,33} However, the electrons display much more complicated phases in QDMs than they are in single-dots. The reason is that in a single QD, electrons have well separated shell structures in energy, and therefore competing phases are far away from the ground state configurations.^{32,33} In contrast, the electrons single-particle energies vary substantially with the inter-dot distance in QDMs. In certain condition, the molecular orbitals may have very close energies (e.g. the σ_u and π_u orbitals), therefore Coulomb energies and correlation effects may play more important roles and lead to various possible phases.

Ota *et al* measured the addition energies of vertically

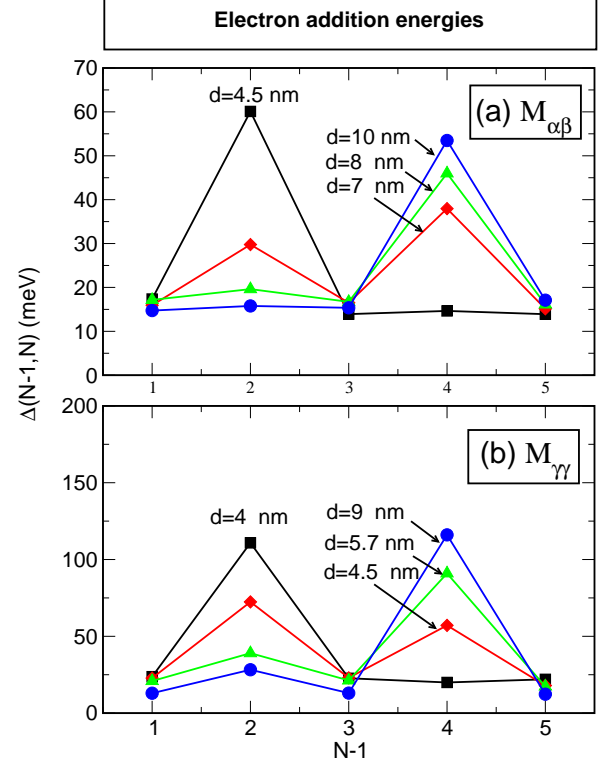
FIG. 11: (Color online) Addison energy $\Delta(N-1, N)$ of $N=1$ - 6 electrons, for (a) hetero-QDMs $M_{\alpha\beta}$ at inter-dot distance $d=4.5$, 7, 8 10 nm, and (b) homo-QDMs $M_{\gamma\gamma}$ at $d=4$, 4.5, 5.7, 9 nm.

TABLE II: Measured Electron addition energies (in meV) of vertically coupled InAs/GaAs quantum dots. The values are extracted from Ref. 19 at zero magnetic field.

	$\Delta(1, 2)$	$\Delta(2, 3)$	$\Delta(3, 4)$	$\Delta(4, 5)$	$\Delta(5, 6)$
$d=6.5$ nm	8	12	6	5	6
$d=11.5$ nm	6	9	3.75	8.25	4.5

coupled quantum dots.¹⁹ The values of these addition energies are extracted and listed in Tab. II. To compare with the experiment, we further calculate the addition energies for $N=1$ - 6 electrons. The addition energies was calculated in a zero field ($E=0$). In principle the electric field may play important role in the addition energies of QDM, due to the large distance between the top

and bottom dots. However, in the experimental setups, the electric field is very small, and should not affect the results.³⁴ We plot the addition energies for QDMs $M_{\alpha\beta}$ and $M_{\gamma\gamma}$ in Figs. 11(a) and 11(b) respectively, for a few inter-dot distances. We see the following features of the addition energies in $M_{\alpha\beta}$:

(i) At short inter-dot distance $d = 4.5$ nm, there is only one addition energy peak at $N - 1=2$. This feature is the same as what we see in a single dot charging.³³ Due to strong coupling between two dots at this inter-dot distance, the electronic structure of the QDM resemble that of a single dot.

(ii) At large inter-dot distance $d = 10$ nm, there is also only one addition energy peak, however it occurs at $N-1=4$. At this inter-dot distance, the coupling between two dots is very small, so the electronic structure of the QDM is very similar to that of two isolated dots.

(iii) At intermediate inter-dot distance $d = 7, 8$ nm, we see two addition energy peaks at $N - 1=2$ and $N - 1=4$ respectively. This feature is not seen in the isolated dots, indicating that new molecular phases emerge in these cases.

Similar features are also seen in $M_{\gamma\gamma}$ [Fig. 11(b)]. Experimentally, when two dots are close ($d \sim 6.5$ nm), the addition energies have one peak, while at $d \sim 11.5$ nm, two addition energy peaks are observed.¹⁹ Therefore, our calculations agree qualitatively with the experiments. However, the calculated addition energies are about 3 times larger than what obtained experimentally. The reasons that might cause the disagreement are (i) the uncertainty of the dot sizes in the experiments;³⁴ (ii) the possible existence of compensating electric field that was not considered in the experiments.

VII. SUMMARY

We have studied the electronic structures of quantum dot molecules made of (In,Ga)As/GaAs dots of different

sizes (hetero-QDMs), and compare them to that of quantum dot molecules made of identical dots (homo-QDMs). We found that while the hetero-QDMs and homo-QDMs have relatively similar electronic structures at short inter-dot distance, they differ significantly at large inter-dot distance. (i) Unlike those of homo-QDMs, the single-particle molecular orbitals of hetero-QDMs convert to dot localized orbitals at large inter-dot distance. (ii) Consequently, the bonding-antibonding splitting of molecular orbitals is significantly larger than the electron hopping energy in a hetero-QMD at large inter-dot distance, whereas for homo-QDM, the bonding-antibonding splitting is very similar to the hopping energy. (iii) The asymmetry of the QDM will significantly increase the double occupation for the two-electron ground states, and therefore affect the degree of entanglement of the two electrons. We also calculate the electron addition energies in QDMs. The addition energy $\Delta(N - 1, N)$ as a function of N show only one peak in strong and weak coupling region at $N - 1= 2, 4$ respectively, while in intermediate coupling region both addition energy peaks are seen. Further examination of the many-particle ground states show that electrons have different configurations in these three regions.

Acknowledgments

L. He acknowledges the support from the Chinese National Fundamental Research Program, the Innovation funds and “Hundreds of Talents” program from Chinese Academy of Sciences, and National Natural Science Foundation of China (Grant No. 10674124). The work done at NREL was funded by the U.S. Department of Energy, Office of Science, Basic Energy Science, Materials Sciences and Engineering, LAB-17 initiative, under Contract No. DE-AC36-99GO10337 to NREL.

¹ Q. Xie, A. Madhukar, P. Chen, and N. P. Kobayashi, Phys. Rev. Lett. **75**, 2542 (1995).

² G. S. Solomon, J. A. Trezza, A. F. Marshall, and J. S. Harris, Phys. Rev. Lett. **76**, 952 (1996).

³ M. Bayer, P. Hawrylak, K. Hinzer, S. Fafard, M. Korkusinski, Z. R. Wasilewski, O. Stern, and A. Forchel1, Science **291**, 451 (2001).

⁴ D. Loss and D. P. DiVincenzo, Phys. Rev. A **57**, 120

(1998).

⁵ J. R. Petta, A. C. Johnson, C. M. Marcus, M. P. Hanson, and A. C. Gossard, Phys. Rev. Lett. **93**, 186802 (2004).

⁶ A. C. Johnson, J. R. Petta, C. M. Marcus, M. P. Hanson, and A. C. Gossard, Phys. Rev. B **72**, 165308 (2005).

⁷ G. Bester, J. Shumway, and A. Zunger, Phys. Rev. Lett. **93**, 047401 (2004).

⁸ L. He, G. Bester, and A. Zunger, Phys. Rev. B **72**,

081311(R) (2005).

⁹ L. He, G. Bester, and A. Zunger, Phys. Rev. B **72**, 195307 (2005).

¹⁰ M. C. Bödefeld, R. J. Warburton, K. Karrai, J. P. Kotthaus, G. Medeiros-Ribeiro, and P. M. Petroff, Appl. Phys. Lett. **74**, 1839 (1999).

¹¹ E. A. Stinaff, M. Scheibner, A. S. Bracker, I. V. Ponomarev, V. L. Korenev, M. E. Ware, M. F. Doty, T. L. Reinecke, and D. Gammon, Science **311**, 636 (2006).

¹² P. N. Keating, Phys. Rev. **145**, 637 (1966).

¹³ J. L. Martins and A. Zunger, Phys. Rev. B **30**, R6217 (1984).

¹⁴ A. J. Williamson, L.-W. Wang, and A. Zunger, Phys. Rev. B **62**, 12963 (2000).

¹⁵ L.-W. Wang and A. Zunger, Phys. Rev. B **59**, 15806 (1999).

¹⁶ A. Franceschetti, H. Fu, L.-W. Wang, and A. Zunger, Phys. Rev. B **60**, 1819 (1999).

¹⁷ M. Rontani, F. Troiani, U. Hohenester, and E. Molinari, Solid State Comm. **119**, 309 (2001).

¹⁸ C. Edmiston and K. Ruedenberg, Rev. Mod. Phys. **35**, 457 (1963).

¹⁹ T. Ota, M. Rontani, S. Tarucha, Y. Nakata, H. Z. Song, T. Miyazawa, T. Usuki, M. Takatsu, and N. Yokoyama, Phys. Rev. Lett. **95**, 236801 (2005).

²⁰ M. A. Nielsen and I. L. Chuang, *Quantum Computation and Quantum Information* (Cambridge University Press, Cambridge, 2000).

²¹ C. H. Bennett, H. J. Bernstein, S. Popescu, and B. Schumacher, Phys. Rev. A **53**, 2046 (1996).

²² C. H. Bennett, D. P. DiVincenzo, J. A. Smolin, and W. K. Wootters, Phys. Rev. A **54**, 3824 (1996).

²³ A. Wehrl, Rev. Mod. Phys. **50**, 221 (1978).

²⁴ J. Schliemann, J. I. Cirac, M. Kuš, M. Lewenstein, and D. Loss, Phys. Rev. A **64**, 022303 (2001).

²⁵ R. Paškauskas and L. You, Phys. Rev. A **64**, 042310 (2001).

²⁶ Y. S. Li, B. Zeng, X. S. Liu, and G. L. Long, Phys. Rev. A **64**, 054302 (2001).

²⁷ P. Zanardi, Phys. Rev. A **65**, 042101 (2002).

²⁸ Y. Shi, Phys. Rev. A **67**, 24301 (2003).

²⁹ H. M. Wiseman and J. A. Vaccaro, Phys. Rev. Lett. **91**, 097902 (2003).

³⁰ G. C. Ghirardi and L. Marinatto, Phys. Rev. A **70**, 012109 (2004).

³¹ C. N. Yang, Rev. Mod. Phys. **34**, 694 (1962).

³² L. He, G. Bester, and A. Zunger, Phys. Rev. Lett. **95**, 246804 (2005).

³³ L. He and A. Zunger, Phys. Rev. B **73**, 115324 (2006).

³⁴ T. Ota, private communication.